Determination of Mean Cumulus Cloud Vorticity from GATE A/B-Scale Potential Vorticity Budget

LAWRENCE CHENG,[1] TSOI-CHING YIP AND HAN-RU CHO

Department of Physics, University of Toronto, Toronto, Ontario, Canada M5S 1A7

(Manuscript received 21 August 1979, in final form 3 December 1979)

ABSTRACT

The effects of cumulus clouds on the large-scale potential vorticity field are investigated using GATE data. Clouds are found to modify the mean potential vorticity field not only through vertical mixing but also through the generation of potential vorticity by the release of latent heat. Overall, the dynamic effect and the thermodynamic effect of clouds are found to contribute about equally to the large-scale potential vorticity budget.

A diagnostic method is also developed to determine mean cloud vertical vorticity profiles from observed large-scale potential vorticity sources. The method is applied to GATE A/B-scale potential vorticity budgets. The results show that 1) the mean cloud vorticity is of the same order of magnitude as the large-scale mean vorticity, despite the smallness of the horizontal scales of cumulus clouds, and 2) the mean cloud vorticity is smaller than the large-scale mean vorticity in the mean detrainment layer of the cloud population, and larger than the large-scale mean vorticity in the mean cloud entrainment layer. These properties are in agreement with the theoretical analysis presented in Cho *et al.* (1979a).

1. Introduction

The effects of cumulus clouds on the large-scale vorticity field have been studied by quite a few investigators. Observationally, Yanai and Nitta (1967) analyzed the large-scale vorticity budget of a Caribbean easterly wave. Reed and Johnson (1974) determined the vorticity budget of a composite easterly wave in the western Pacific. Williams and Gray (1973) and Ruprecht and Gray (1976) have studied the vorticity budgets of composite cloud clusters. Vorticity budget analyses using GATE data have been made by Stevens (1979) and Reeves *et al.* (1979).

Several theoretical attempts have been made to interpret the observed cloud effects on the large-scale vorticity field. Reed and Johnson (1974) studied the effects of vertical eddy advection due to cumulus convection. Shapiro (1978) proposed a formulation in which a cloud twisting effect was included. Cho *et al.* (1979a) presented a formulation through which the cloud eddy advection and eddy tilting processes can be described completely in terms of the total cloud mass flux alone. Most recently, Cho and Cheng (1979) suggested that horizontal eddy transport of vorticity by cumulus clouds could be a very important component in the large-scale vorticity budget.

An alternative approach to this problem using the concept of potential vorticity has been suggested by Fraedrich (1974). The major advantage of this approach lies in the fact that potential vorticity satisfies a conservation equation which is much simpler in form than that of vorticity. However, a number of assumptions have been made either implicitly or explicitly by the author. The real advantage of the potential vorticity approach may not be so clear if some of these assumptions cannot be justified.

One of the purposes of this paper is to present a rigorous formulation of cloud effects in the large-scale potential vorticity equation, to investigate the validity of some of the simplification assumptions made by the earlier investigators, and hence to study the feasibility of using the concept of potential vorticity to parameterize the effects of cumulus clouds on the large-scale vorticity field.

The second purpose of this study is to develop a set of budget equations which can be used to determine the values of mean cloud vorticity from observed large-scale potential vorticity budgets. The results can be useful in many theoretical as well as diagnostic studies. For example, the mean cloud vorticity values deduced in this study can be used to verify some of the theoretical conclusions reached by Cho *et al.* (1979a). They have also been used by Cho and Cheng (1979) to evaluate the effects of cloud horizontal transport of vorticity.

GATE data have been used in this investigation. The A/B-scale heat, moisture and potential vorticity budgets have been analyzed for two 1-day periods (0000–2400 GMT 2 September and 0000–2400 GMT 9 September) during Phase III of GATE. These ob-

[1] Present affiliation: Atmospheric Sciences Division, Alberta Research Council, Edmonton, Alberta, Canada.

0022-4928/80/040797-14$07.50

served budget results form the observational basis for this investigation.

2. The large-scale potential vorticity equation

The potential vorticity will be defined in this paper as

$$\chi = -\zeta_a \cdot \nabla\theta/\rho g, \tag{1}$$

where θ is the potential temperature, ζ_a the three-dimensional absolute vorticity vector, ρ the air density, ∇ the three-dimensional gradient operator and g the gravitational acceleration. Since the variations in air density ρ, even inside cumulus clouds, is only about a few percent of its background mean values, the mean air density $\bar{\rho}$ will be used to replace ρ in Eq. (1). For convenience, we shall use η to denote the vertical component of ζ_a and the vector ξ to denote its horizontal components.

According to Ertel's theorem, the conservation equation for the potential vorticity, including the latent heating and the radiative heating effects, can be written as

$$\frac{\partial\chi}{\partial t} + \nabla_H \cdot \mathbf{v}\chi + \frac{\partial\omega\chi}{\partial p} = \frac{-1}{\rho g}\nabla_H \cdot \{\xi[L(c-e) + Q_R]/C_p\pi\} + \frac{\partial}{\partial p}\{\eta[L(c-e) + Q_R]/C_p\pi\}. \tag{2}$$

∇_H is used in the above equation to denote the two-dimensional horizontal gradient operator. C is the rate of condensation of water vapor and e the rate of evaporation of liquid water. L is the latent heat of vaporization, Q_R the radiative heating rate, $\pi = (p/1000)^{R/C_p}$ the nondimensional pressure and ω the vertical p-velocity.

The large-scale mean potential vorticity will be defined as

$$\bar{\chi} = -\bar{\zeta}_a \cdot \nabla\bar{\theta}/\bar{\rho} g. \tag{3}$$

The overbar is used to denote the large-scale area average. The following equation usually gives a good approximation for the mean potential vorticity:

$$\bar{\chi} = -\frac{\partial\bar{v}}{\partial\rho}\frac{\partial\bar{\theta}}{\partial x} + \frac{\partial\bar{u}}{\partial p}\frac{\partial\bar{\theta}}{\partial y} + \left(\frac{\partial\bar{v}}{\partial x} - \frac{\partial\bar{u}}{\partial y} + f\right)\frac{\partial\bar{\theta}}{\partial p}. \tag{4}$$

Here f is the Coriolis parameter, and u and v are the eastward and northward components of horizontal air velocity.

A horizontal area average of Eq. (2) gives the large-scale potential vorticity equation

$$\frac{\partial\bar{\chi}}{\partial t} + \nabla_H \cdot \bar{\mathbf{v}}\bar{\chi} + \frac{\partial\bar{\omega}\bar{\chi}}{\partial p} = -\frac{1}{\bar{\rho} g}\nabla_H \cdot (\bar{\xi}\bar{Q}_R/C_p\pi) + \frac{\partial}{\partial p}(\bar{\eta}\bar{Q}_R/C_p\pi) - \frac{1}{g\bar{\rho}}\nabla_H \cdot \{\overline{\xi[L(c-e)/C_p\pi]}\} + \frac{\partial}{\partial p}\{\overline{\eta[L(c-e)/C_p\pi]}\} - \frac{\partial}{\partial p}(\overline{\omega\chi} - \bar{\omega}\bar{\chi}) - \nabla_H \cdot (\overline{\mathbf{v}'\chi'}). \tag{5}$$

The assumption has been made that the eddy correlation terms between vorticity and radiative heating rate is small and can be neglected. It can be justified by comparing the eddy radiative heating terms $\nabla_H \cdot (\overline{\xi' Q_R'/C_p\pi})$ and $\partial(\overline{\eta' Q_R'/C_p\pi})/\partial p$ with the terms due to condensation and evaporation $\nabla_H \cdot \{\overline{\xi[L(c-e)/c_p\pi]}\}$ and $\partial\{\overline{\eta[L(c-e)/C_p\pi]}\}/\partial p$. The mean radiative heating rate $\bar{Q}_R$ is usually one order of magnitude smaller than the mean condensation minus evaporation rate $L(\bar{c} - \bar{e})$ under intensely convective weather conditions. In order that the eddy radiative heating terms be important, Q_R inside clouds has to be comparable in magnitude with $L(c - e)$ in the clouds. This is highly unlikely.

The last four terms on the right-hand side of (5) are due to the presence of cumulus clouds. The net cloud and radiation effects in the large-scale potential vorticity equation will be referred to as the apparent vorticity source Z_1, which is defined as

$$Z_1 = \frac{\partial\chi}{\partial t} + \nabla_H \cdot \bar{\mathbf{v}}\bar{\chi} + \frac{\partial\bar{\omega}\bar{\chi}}{\partial p}. \tag{6}$$

3. The vertical eddy flux of potential vorticity

The potential vorticity defined in (1) is a composite variable. The eddy flux $(\overline{\omega\chi} - \bar{\omega}\bar{\chi})$ of potential vorticity, consequently, has a rather complex expression:

$$\overline{\omega\chi} - \bar{\omega}\bar{\chi} = -\frac{1}{\rho g}[\bar{\omega}\overline{\zeta_a' \cdot \nabla\theta'} + \overline{\omega'\zeta_a'} \cdot \nabla\bar{\theta} + \bar{\zeta}_a \cdot \overline{\omega'\nabla\theta'} + \overline{\omega'\zeta_a' \cdot \nabla\theta'}]. \tag{7}$$

It contains a triple correlation term. The representation of this eddy flux in terms of the collective properties of the cumulus population therefore requires careful consideration. The basic approach used to derive this representation will be that developed by Cho (1977).

In the formulation introduced by Cho, finite life spans of individual cumulus clouds are taken into consideration explicitly. Clouds are classified according to the pressure p' at the maximum cloud-top height reached by a cloud. A cloud population is described by a cloud distribution function $f(\tau,p')$ which is a function of maximum cloud-top pressure

p' as well as cloud age τ. $f(\tau,p')$ is defined in such a way that $f(\tau_0,p_0')\Delta\tau\Delta p$ gives the fractional area covered by clouds with maximum cloud top height $p_0' - \Delta p/2 \leqslant p' < p_0' + \Delta p/2$ and cloud age $\tau_0 - \Delta\tau/2 \leqslant \tau < \tau_0 + \Delta\tau/2$. The notation $\tau_{p'}$ will be used to denote the life span of clouds with maximum cloud-top height p'. The fractional area covered by clouds with maximum cloud-top height p' is thus given by

$$\sigma(p') = \int_0^{\tau_{p'}} f(\tau,p')d\tau \tag{8}$$

and the total fractional cloud coverage $\sum$ can be computed according to

$$\sum = \int \sigma(p')dp'. \tag{9}$$

It has been shown (Cho, 1977) that

$$f(\tau, p') \approx \sigma(p')/\tau_{p'}. \tag{10}$$

Using this cloud distribution function, the average of a meteorological variable, say α, can be written as

$$\bar{\alpha} = \int f(\tau, p')\alpha_c d\lambda + (1 - \textstyle\sum)\tilde{\alpha}. \tag{11}$$

We have used $d\lambda$ to denote $d\tau dp'$ for simplicity. The multiple integral in the averaging has been replaced by a simple integral sign. The proper integration limits have also been dropped for convenience. The subscript c is used to denote values of α at points inside clouds and $\tilde{\alpha}$ is used to denote the mean value of α in the cloud environment. From (11), $\tilde{\alpha}$ may also be expressed in terms of $\bar{\alpha}$ and α_c, i.e.,

$$\tilde{\alpha} = \left[\bar{\alpha} - \int f(\tau, p')\alpha_c d\lambda\right](1 - \textstyle\sum)^{-1}. \tag{12}$$

Application of (11) to $\omega\chi$ gives

$$\overline{\omega\chi} = \int f\omega_c\chi_c d\lambda + (1 - \textstyle\sum)\tilde{\omega}\tilde{\chi}, \tag{13}$$

where $\tilde{\chi}$ is given by

$$\tilde{\chi} = -\tilde{\zeta}_a\cdot\nabla\tilde{\theta}/\tilde{\rho}g. \tag{14}$$

The assumption that $\widetilde{\omega X} = \tilde{\omega}\tilde{X}$ has also been made. Combining Eqs. (12), (13) and (14) one obtains readily that

$$\overline{\omega\chi} = \int f\omega_c\chi_c d\lambda - \frac{1}{\rho g}\left(\bar{\omega} - \int f\omega_c d\lambda\right)\left(\nabla\bar{\theta} - \int f(\nabla\theta)_c d\lambda\right)\cdot\left(\bar{\zeta}_a - \int f\zeta_{ac}d\lambda\right)(1 - \textstyle\sum)^{-2}. \tag{15}$$

$\sum$ is generally of the order of 10^{-1}–10^{-2}. The denominator of the second term on the right-hand side of the above equation may be replaced by unity, and the equation may be further expanded to give

$$\overline{\omega\chi} - \bar{\omega}\bar{\chi} = \int f\omega_c(\chi_c - \bar{\chi})d\lambda + \frac{1}{\bar{\rho}g}\int f\tilde{\omega}\tilde{\zeta}_a\cdot(\nabla\theta)_c d\lambda + \frac{1}{\bar{\rho}g}\int f\tilde{\omega}\nabla\bar{\theta}\cdot\zeta_{ac}d\lambda + O(\textstyle\sum^2). \tag{16}$$

Here $O(\sum^2)$ is used to denote terms of the second or higher orders in $\sum$. Since $\sum$ is very small, these terms may be neglected without introducing any serious errors.

We note that $\tilde{\omega}$ is usually two orders of magnitude smaller than ω_c. The second and third terms on the right-hand side of (16) can be neglected provided that

$$\int f(\nabla\theta)_c d\lambda \leqslant \textstyle\sum \nabla\bar{\theta}, \tag{17}$$

$$\int f\zeta_{ac}d\lambda \leqslant \textstyle\sum \tilde{\zeta}_a. \tag{18}$$

To prove Eq. (17), we first note that the vertical components of $(\nabla\theta)_c$ and $\nabla\bar{\theta}$ are usually comparable in magnitude. Therefore,

$$\int f\frac{\partial\theta_c}{\partial p}d\lambda \sim \sum\frac{\partial\bar{\theta}}{\partial p}.$$

As to the horizontal components, we consider the area averages of θ and $\nabla_H\theta$, i.e.,

$$\bar{\theta} = \int f\theta_c d\lambda + (1 - \textstyle\sum)\tilde{\theta}, \tag{19}$$

$$\overline{\nabla_H\theta} = \int f(\nabla_H\theta)_c d\lambda + (1 - \textstyle\sum)\widetilde{\nabla_H\theta}. \tag{20}$$

$\widetilde{\nabla_H\theta}$ may be considered equal to $\nabla_H\tilde{\theta}$ if one assumes that θ has little fluctuations in the cloud environment. Since

$$\nabla_H\bar{\theta} = \overline{\nabla_H\theta}$$

one obtains

$$\int f(\nabla_H\theta)_c d\lambda = \nabla_H\int f\theta_c d\lambda - (\nabla_H\textstyle\sum)\tilde{\theta} = \textstyle\sum\nabla_H\tilde{\theta}_c + (\nabla_H\textstyle\sum)(\tilde{\theta}_c - \tilde{\theta}), \tag{21}$$

where $\tilde{\theta}_c$, the mean cloud potential temperature, is defined as

$$\tilde{\theta}_c = \int f\theta_c d\lambda \Big/ \textstyle\sum. \tag{22}$$

Both terms on the right-hand side of (21) are comparable in magnitude with $\sum \nabla_H \bar{\theta}$. One concludes therefore that

$$\int f(\nabla_H \theta)_c d\lambda \sim \sum \nabla_H \bar{\theta}.$$

This then completes the proof for Eq. (17).

Eq. (18) follows directly from

$$\xi_c = O(\bar{\xi}),$$
$$\overline{\eta_c} = O(\bar{\eta}).$$

$\bar{\eta}_c$ is used to denote the values of η_c averaged over areas occupied by clouds. The first of the above two equations follows from a simple dimensional argument. With a typical vertical wind shear, the horizontal component of the large-scale mean vorticity is of the order 10^{-3} s^{-1}. The horizontal component of the cloud-scale vorticity for typical cloud horizontal and vertical velocities has generally a comparable magnitude. The proof for the second of the above equations, however, is somewhat involved and has been given by Cho *et al.* (1979a). It will therefore not be repeated here. Since in this paper the vertical component of the mean cloud vorticity will be determined diagnostically from the observed large-scale potential vorticity budget, the validity of this point may also be verified *a posteriori*.

With Eqs. (17) and (18), one finally concludes that the vertical eddy flux of potential vorticity can be expressed in a rather simple form

$$\overline{\omega\chi} - \bar{\omega}\bar{\chi} = \int f\omega_c(\chi_c - \bar{\chi})d\lambda. \tag{23}$$

It is actually identical in form with the cumulus eddy heat and moisture fluxes derived by many earlier authors (Ooyama, 1971; Arakawa and Schubert, 1974; Yanai *et al.*, 1973).

4. Horizontal eddy flux of potential vorticity

In theories of cumulus parameterization, horizontal eddy fluxes of air properties produced by cumulus convection are usually neglected. However, Cho and Cheng (1979) suggested that while this assumption is generally valid for the heat and moisture fluxes, it cannot be applied to the vorticity field. These authors found from both theoretical as well as observational considerations that horizontal eddy transport of vorticity by cumulus convection could be a very significant component in the vorticity budgets of large-scale tropical weather systems. The dynamic processes responsible for this horizontal eddy transport of vorticity have been discussed in their paper.

Due to the lack of a detailed knowledge of the structure of cloud-scale potential vorticity fields, it is not clear at present whether clouds can produce significant horizontal transport of potential vorticity. However, the concept of potential vorticity is closely associated with vorticity. Because of the possible generation of cloud potential vorticity by the latent heating processes, the potential vorticity at a point inside a cloud could be one to two orders larger than its large-scale mean value. The possibility does exist that the cloud horizontal transport of potential vorticity could be significant. In order to keep our formulation as general as possible, the effect of horizontal eddy transport will be included in this paper. The condition under which the effect may be small will be discussed. Diagnostic results both with and without this effect will be presented for comparison.

It has been shown in Cho and Cheng (1979) that, for any meteorological variable α, the divergence of horizontal eddy flux of α caused by clouds is given by

$$\nabla_H \cdot \overline{(\mathbf{v}'\alpha')} = \frac{\partial M_c}{\partial p}(\bar{\alpha}_{cB} - \bar{\alpha}). \tag{24}$$

Here M_c is the total cloud mass flux

$$M_c = -\int f\omega_c d\lambda \tag{25}$$

and $\bar{\alpha}_{cB}$ is a weighted mean value of α around cloud boundaries defined in the following sense:

$$\int f\nabla_H \cdot (\mathbf{v}_c\alpha_c)d\lambda = \frac{\partial M_c}{\partial p}\bar{\alpha}_{cB}. \tag{26}$$

Applying (24) to the potential vorticity one finds the divergence of horizontal eddy flux of potential vorticity is given by

$$\nabla_H \cdot \overline{(\mathbf{v}'\chi')} = \frac{\partial M_c}{\partial p}(\bar{\chi}_{cB} - \bar{\chi}). \tag{27}$$

A necessary and sufficient condition for small effects of horizontal eddy transport of potential vorticity can now be found from Eq. (27). The effects of horizontal eddy transport is negligibly small if and only if the mean value of potential vorticity around cloud boundaries is approximately equal to its large-scale mean, i.e.,

$$\bar{\chi}_{cB} \approx \bar{\chi}. \tag{28}$$

This condition will be used later in this paper to eliminate the effects of horizontal eddy transport of potential vorticity. Diagnostic results both with and without the effect of horizontal eddy transport will be presented.

5. Representation of cloud effects in the large-scale mean potential vorticity equation

Combining Eqs. (5), (6), (16) and (27), together with the cloud potential vorticity equation

$$\frac{\partial \chi_c}{\partial t} + \nabla_H \cdot \mathbf{v}_c \chi_c + \frac{\partial \omega_c \chi_c}{\partial p} = -\frac{1}{\bar{\rho} g} \nabla_H \cdot [\xi_c L(c - e)/C_p \pi] + \frac{\partial}{\partial p} [\eta_c L(c - e)/C_p \pi], \quad (29)$$

a parameterized form of the apparent potential vorticity source can now be derived:

$$Z_1 + \frac{1}{\bar{\rho} g} \nabla_H \cdot (\bar{\xi} \bar{Q}_R / C_p \pi) - \frac{\partial}{\partial p} (\bar{\eta} \bar{Q}_R / C_p \pi) = \int \frac{\sigma(p')}{\tau_{p'}} [\chi_c(\tau_{p'}) - \bar{\chi}] dp' - M_c \frac{\partial \bar{\chi}}{\partial p}. \quad (30)$$

Here $\chi_c(\tau_{p'})$ is the value of χ_c at the end of a cloud life-cycle. The derivation of this equation is very similar to that given by Cho (1977) for heat and moisture budget equations. The details will not be repeated here except to mention that in the derivation a cloud area is defined as the region of the atmosphere above the cloud-base level that is not in hydrostatic balance with the mean environment. According to this definition, both condensation as well as evaporation processes are considered to be realized mainly inside clouds.

The first terms on the right-hand side of Eq. (30) represent the cloud life-cycle effect discussed in Cho (1977). The second term represents the vertical advection of mean potential vorticity by cumulus mass flux. A detailed evaluation of the cloud life-cycle effect requires a three-dimensional time-dependent cloud model as well as a knowledge of the cloud distribution function. As a first attempt, we do not intend to introduce the spectrum representation of clouds by using a time-dependent cloud model. Instead, the cloud life-cycle effect will be simply described in terms of an ensemble mean cloud potential vorticity $\bar{\chi}_c$ defined by the relationship

$$\int \frac{\sigma(p')}{\tau_{p'}} [\chi_c(\tau_{p'}) - \bar{\chi}] dp' = \left[\int \frac{\sigma(p')}{\tau_{p'}} dp' \right] (\bar{\chi}_c - \bar{\chi}). \quad (31)$$

The meaning of the integral on the right-hand side of this equation has been discussed by Cho (1977). It may be referred to as the recycling rate of the atmospheric air by cumulus convection.

6. Budget equations for the determination of ensemble mean cloud vorticity

We note from the right-hand side of (5) that release of latent heat by cumulus clouds modifies the mean potential vorticity field. The rate of this modification depends on the values of cloud vorticity. This relationship provides the possibility to determine cloud vorticities from the observed apparent vorticity source. The set of budget equations that can be used for this purpose will be derived in this section. Since we do not intend to introduce cloud spectrum decomposition for lack of a proper cloud model, only ensemble mean equations for the cloud population as a whole will be derived. In this respect, the method discussed here is very similar to the bulk method introduced by Yanai *et al.* (1973) for the large-scale heat and moisture budget equations.

The cloud potential vorticity equation (29), when multiplied by the cloud distribution function $f(\tau,p')$ and averaged over the cumulus cloud population, gives

$$\int \frac{\sigma}{\tau_{p'}} (\chi_c(\tau_{p'}) - \bar{\chi}) dp' + \frac{\partial M_c}{\partial p} \bar{\chi}_{cB} - \frac{\partial M_c \bar{\chi}_c}{\partial p} = \frac{\partial}{\partial p} [\bar{\eta}_c L(\bar{c} - \bar{e})/C_p \pi]. \quad (32)$$

Note that the horizontal components of the cloud vorticity do not appear on the right-hand side of the above equation. When averaged over a cloud cross-sectional area

$$\int_a \nabla_H \cdot [\xi_c L(c - e)/C_p \pi] da = \oint \frac{L}{C_p \pi} (c - e) \xi_c \cdot \hat{\mathbf{n}} dl. \quad (33)$$

The line integral is performed around the boundary of a cloud, and $\hat{\mathbf{n}}$ is the unit vector normal to the cloud boundary. Since we have assumed in this formulation (following Cho, 1977) that condensation and evaporation processes are mostly realized inside clouds, $(c - e)$ should approach zero near the cloud edge and the integral vanishes. $\bar{\eta}_c$ in Eq. (32) is the ensemble mean of the vertical component of cloud vorticity. The equation relates $\bar{\eta}_c$ to other collective properties of the cumulus cloud population. When combined with Eq. (30), Eq. (32) may also be written as

$$Z_1 + \frac{1}{\bar{\rho} g} \nabla_H \cdot (\bar{\xi} \bar{Q}_R / C_p \pi) - \frac{\partial}{\partial p} (\bar{\eta} \bar{Q}_R / C_p \pi) + \frac{\partial M_c}{\partial p} \bar{\chi}_{cB} - \frac{\partial M_c \bar{\chi}_c}{\partial p} + M_c \frac{\partial \bar{\chi}}{\partial p} = \frac{\partial}{\partial p} [\bar{\eta}_c L(\bar{c} - \bar{e})/C_p \pi]. \quad (34)$$

This equation may be used to determine $\bar{\eta}_c$ from an observed Z_1 profile, provided that M_c, $\bar{\chi}_c$, $\bar{\chi}_{cB}$ and $(\bar{c} - \bar{e})$ are known.

The mean condensation minus evaporation rate

may be determined from the large-scale heat and moisture budget equations. These equations, when written in terms of the dry static energy $s = C_pT + gz$ and water vapor mixing ratio q, can be expressed as

$$Q_1 = \frac{\partial \bar{s}}{\partial t} + \nabla_H \cdot \bar{\mathbf{v}}\bar{s} + \frac{\partial \bar{\omega}\bar{s}}{\partial p} = L(\bar{c} - \bar{e}) - \frac{\overline{\partial \omega' s'}}{\partial p} + Q_R, \quad (35)$$

$$Q_2 = -L\left(\frac{\partial \bar{q}}{\partial p} + \nabla_H \cdot \bar{\mathbf{v}}\bar{q} + \frac{\partial \bar{\omega}\bar{q}}{\partial p}\right) = L(\bar{c} - \bar{e}) + L\frac{\overline{\partial \omega' q'}}{\partial p}. \quad (36)$$

Q_1 and Q_2 are conventionally referred to as the apparent heat source and the apparent moisture sink, respectively. It has been shown (Yanai *et al.*, 1973; Arakawa and Schubert, 1974; Cho, 1977) that

$$Q_1 - Q_R = -M_c \frac{\partial \bar{s}}{\partial p}, \quad (37)$$

$$Q_2 = -\left(\int \frac{\sigma}{\tau_{p'}} dp'\right)(\bar{q}^* - \bar{q}) + M_c \frac{\partial \bar{q}}{\partial p}, \quad (38)$$

where q^* is the saturation water vapor mixing ratio.

We shall assume in this study that (e.g., Yanai *et al.*, 1973; Ogura and Cho, 1973)

$$\overline{\omega' s'} = -M_c(\bar{s}_c - \bar{s}), \qquad \overline{\omega' q'} = -M_c(\bar{q}_c - \bar{q}). \quad (39)$$

Since M_c in this formulation includes both cloud updrafts as well as evaporation-induced cloud downdrafts, $\bar{s}_c$ and $\bar{q}_c$ should be interpreted here as the ensemble mean values of s_c and q_c weighted with respect to the mass fluxes of clouds. Combining Eqs. (35) and (36) yields

$$Q_1 - Q_2 - Q_R = -\frac{\partial \overline{\omega' h'}}{\partial p} = \frac{\partial}{\partial p}[M_c(\bar{h}_c - \bar{h})]. \quad (40)$$

Here $h = s + Lq$ is the moist static energy and $\bar{h}_c$ the mass-flux-weighted mean cloud moist static energy.

The mean cloud moist static energy $\bar{h}_c$ may be related to the mean cloud dry static energy $\bar{s}_c$ if one assumes that the cloud air is mostly saturated (Arakawa and Schubert, 1974):

$$\bar{s}_c - \bar{s} = \frac{1}{1 + \gamma}(\bar{h}_c - \bar{h}^*), \quad (41)$$

where γ is given by

$$\gamma = \frac{L}{C_p}\left(\frac{\partial \bar{q}^*}{\partial \bar{T}}\right)_p$$

and h^* is the saturated moist static energy. The mean condensation minus evaporation rate can then be determined from (35), i.e.,

$$L(\bar{c} - \bar{e}) = Q_1 - Q_R - \frac{\partial}{\partial p}[M_c(\bar{s}_c - \bar{s})]. \quad (42)$$

Given a set of observed Q_1, Q_2 and Q_R profiles, the total cloud mass flux M_c may be determined from (37). With this M_c, the recycling rate can be determined from (38). The mean condensation minus evaporation rate can then be determined from Eq. (42), together with Eqs. (40) and (41).

In order to determine the mean cloud vorticity from (34), one needs to know $\bar{\chi}_c$ and $\bar{\chi}_{cB}$, in addition to cloud thermodynamic properties and the observed Z_1 profile. We shall assume that the ensemble mean $\bar{\chi}_c$ defined in (31), and determined from Z_1 through (30), may be used for the mean cloud potential vorticity $\bar{\chi}_c$ required in the vertical flux $M_c\bar{\chi}_c$. Since the ensemble mean values of χ_c derived from the cloud life-cycle effect may not be exactly the same as that required in computing the vertical flux of potential vorticity using the simple formula $M_c\bar{\chi}_c$, a certain amount of approximation is involved here. The simplification is introduced to make the problem tractable without using a sophisticated three-dimensional cloud model.

As to the value of $\bar{\chi}_{cB}$, three different assumptions will be used and tested:

$$\text{(I)} \quad \bar{\chi}_{cB} = \bar{\chi}_c$$

$$\text{(II)} \quad \bar{\chi}_{cB} = \bar{\chi}$$

$$\text{(III)} \quad \bar{\chi}_{cB} = \begin{cases} \bar{\chi}_c & \text{in mean cloud detrainment layer} \\ \bar{\chi} & \text{in mean cloud entrainment layer.} \end{cases} \quad (43)$$

The third assumption is based on the argument that in the mean cloud detrainment layer cloud air on the average flows out of cloud and it should bring the cloud properties into the cloud environment. On the other hand, in the entrainment layer air converges into cloud and it should carry the environmental properties.

As discussed in Section 4, the second boundary condition given above is equivalent to the assumption that the effects of horizontal eddy transport of potential vorticity are negligibly small. Diagnostic results obtained using this boundary condition will then correspond to the results obtained by neglecting the horizontal eddy flux of potential vorticity in the formulation.

Thus we have developed a closed set of equations which can be used to determine ensemble mean cloud vorticity from observed large-scale heat, moisture and potential vorticity budgets. GATE A/B-scale data have been analyzed to provide the observed Q_1, Q_2 and Z_1 profiles. These observed budgets will be discussed in Section 7.

7. GATE A/B-scale heat, moisture and potential vorticity budgets

The A/B-scale aerological data have been analyzed for two 1-day periods (0000–2400 GMT 2 September and 0000–2400 GMT 9 September) during Phase III of GATE. These analyzed data have previously been used by Cho *et al.* (1979a) and Cho and Cheng (1979) to study the cumulus cloud effects on the A/B-scale vorticity fields. Methods of data analyses have been discussed by these authors. Readers are referred to their papers for details. Analyzed results relevant to potential vorticity budget studies will be presented in this section.

One of the most important synoptic features in GATE during Phase III of the experiment was that a series of easterly waves, originating over western Africa, passed through the GATE network. An excellent chronology of these waves has been presented and discussed in detail by Thompson *et al.* (1979).

According to Thompson *et al.*, the trough region of an easterly wave moved over the GATE A/B-scale network during the period 0000–2400 GMT 2 September. Shipboard rain measurements all reported heavy precipitation. SMS-1 infrared satellite pictures reveal a heavy cloud mass moved into the GATE area from northeast at 0000 GMT. The cloud mass became more intensified and was located almost at the center of the A/B-scale array at 1200 GMT.

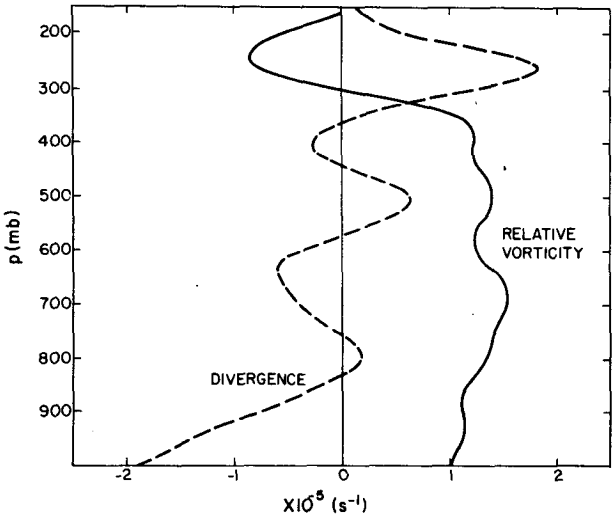

FIG. 1. GATE A/B-scale mean divergence and relative vorticity profiles for the period 0000–2400 GMT 2 September.

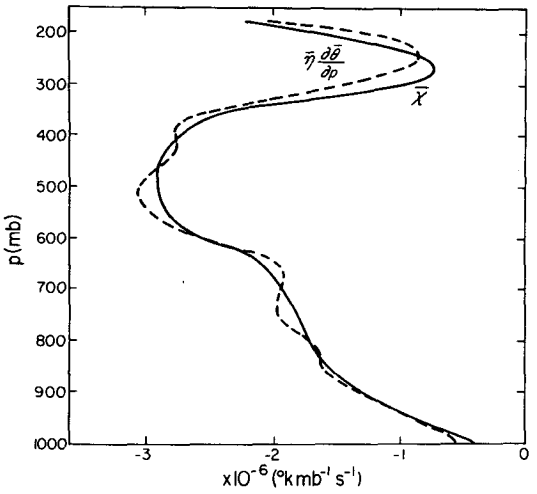

FIG. 2. GATE A/B-scale mean potential vorticity profile for the period 0000–2400 GMT 2 September. The dashed line shows the mean potential vorticity calculated according to Eq. (44) using the vertical vorticity only.

For the second analyzed period, precipitation measurements showed a marked increase in surface precipitation rate starting 1800 GMT 8 September. Based on the study of Thompson *et al.* (1979), the region of maximum northerly wind of an easterly wave entered the GATE observation network at about this time. The trough region of the wave passed through the GATE region during the period 1200–1800 GMT 9 September. SMS-1 IR imagery shows that a heavy cloud mass propagated through the northern portion of the GATE A/B-scale network. Convective activities were very intense during both of the periods analyzed for this study.

a. 2 September period

Fig. 1 shows the vertical profiles of the A/B-scale mean divergence and relative vorticity for the period 0000–2400 GMT 2 September. Both divergence and relative vorticity are of the order 10^{-5} s^{-1}. The divergence profile is characterized by a strong convergence layer below the 800 mb level and a strong divergence layer around 250 mb. Between these two layers there are layers of relatively weak convergence and divergence. Similar complex structures in the divergence profile have also been reported by Nitta (1977) and Thompson *et al.* (1979) for other periods of GATE.

The structure of the relative vorticity profile is characterized by a deep layer of cyclonic vorticity below 300 mb and a thin layer of anticyclonic vorticity above. The distribution of cyclonic vorticity below 300 mb is rather uniform in height.

Fig. 2 shows the mean potential vorticity $\bar{\chi}$

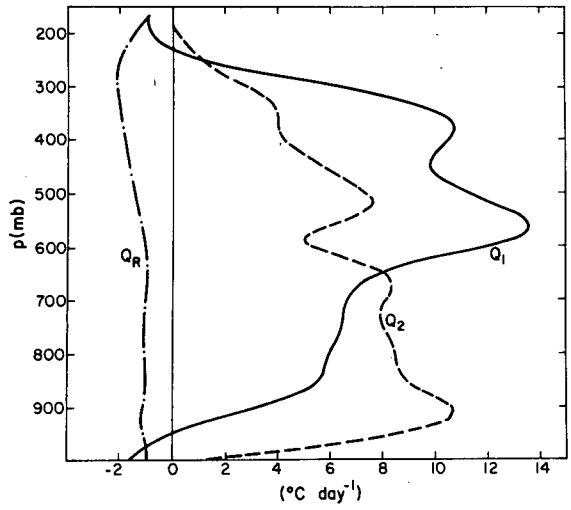

FIG. 3. GATE A/B-scale mean apparent heat source Q_1, apparent moisture sink Q_2, and the radiative heating rate Q_R for the period 0000–2400 GMT 2 September.

(solid line) calculated according to Eq. (4). The mean potential vorticity is negative throughout the depth of the troposphere. Its magnitude reaches a maximum at about 500 mb, and a minimum at about 250 mb. The maximum is due mainly to the strong vertical stability at that level, while the minimum is caused by the decrease in absolute vorticity.

Also shown in the figure (dashed line) is the mean potential vorticity calculated according to

$$\bar{\chi} = \bar{\eta} \frac{\partial \bar{\theta}}{\partial p} . \tag{44}$$

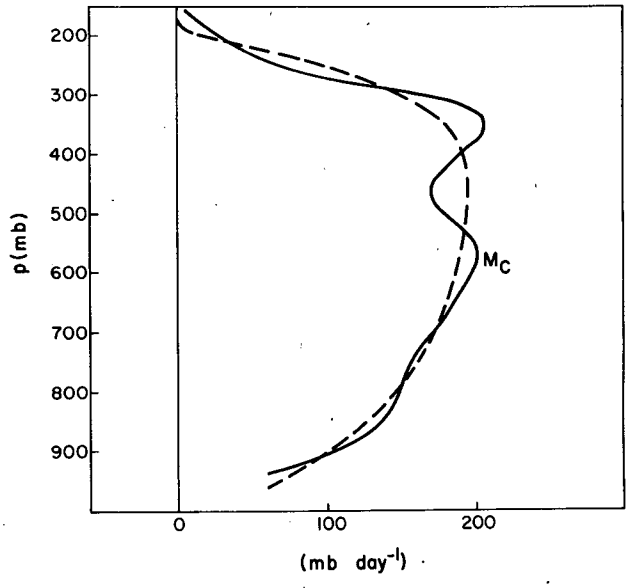

FIG. 4. GATE A/B-scale total cloud mass flux M_c for the period 0000–2400 GMT 2 September.

This simplified expression appears to give a very good approximation for the mean potential vorticity.

The A/B-scale apparent heat source Q_1 and apparent moisture sink Q_2 are shown in Fig. 3. A reliability test of these observed Q_1 and Q_2 has been made and discussed in Cho and Cheng (1979). Also shown in the figure is the A/B-scale mean radiative heating rate Q_R calculated according to the method described by Rogers and Walshaw (1966). Some details of the calculation have been described in Cho *et al.* (1979b).

Using the observed Q_1 and Q_2 profiles, the total cloud mass flux M_c and the recycling rate can be determined from (37) and (38). The M_c determined is shown in Fig. 4. It has a maximum at ~350 mb. Except for a little fluctuation around 450 mb, the value of M_c increases from the cloud-base level up to ~350 mb and decreases rapidly to zero above this level. It is not clear at present whether the small fluctuations in the M_c profile are significant. The dashed line shows a smoothed M_c profile in which these small fluctuations are filtered out. Only the solid M_c curve, however, is used in subsequent calculations. The recycling rate is shown in Fig. 5. Overall, it has a magnitude of the order of 1 day^{-1}. This implies that the atmospheric air is processed by cumulus clouds about once in one day's time. The recycling rate has a rather substantial vertical variation and it has a maximum at ~300 mb. This is probably caused by the vertical variations in cross-sectional areas of clouds. The cross-sectional area of a deep cumulonimbus cloud often shows a large expansion at its upper detrainment layer. The recycling rate profile appears then to suggest that the cloud population has a major detrainment layer at ~300 mb. This is in agreement with the M_c profile shown in Fig. 4. Since M_c decreases rapidly with

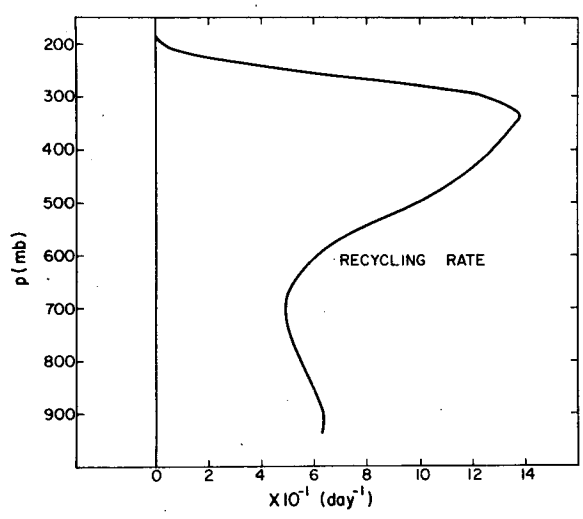

FIG. 5. GATE A/B-scale atmospheric recycling rate by cumulus clouds for the period 0000–2400 GMT 2 September.

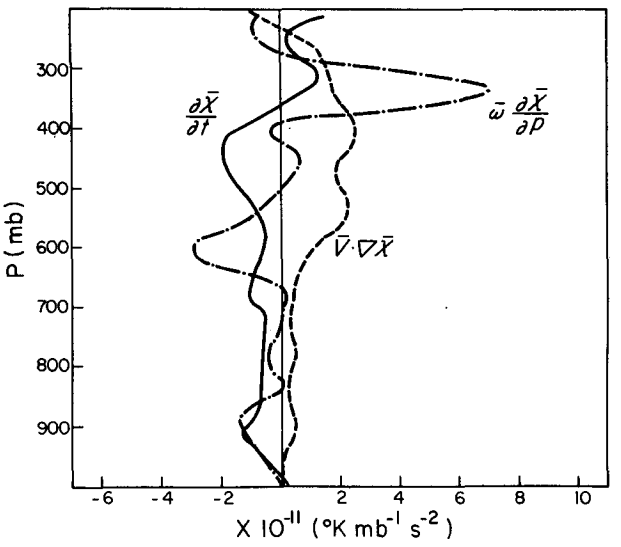

FIG. 6. Vertical profiles of local time rate of change and the horizontal and vertical advections of the A/B-scale mean potential vorticity for the period 0000–2400 GMT 2 September.

height at ~300 mb, the main detrainment layer of clouds should be located at about this level.

The vertical profiles of the local time rate of change and the horizontal and vertical advections of the large-scale mean potential vorticity are shown in Fig. 6. Overall, the three terms contribute about equally to the large-scale mean potential vorticity budget. However, at upper levels around 350 mb the vertical advection of potential vorticity appears to dominate. The values of the mean potential vorticity appear to be decreasing with time below 350 mb and increasing with time above that level. The horizontal advection of mean potential vorticity is positive below 250 mb and negative above. The structure of the profile of vertical advection of potential vorticity is somewhat more complex. There is a maximum at the 350 mb level and a minimum at the 600 mb level. Both of them are caused mainly by the strong local vertical gradient in mean potential vorticity.

The apparent potential vorticity source Z_1 as defined in Eq. (6) is shown in Fig. 7 as the solid line. The figure shows that there is a net apparent potential vorticity sink below 550 mb and above 250 mb. In between these two levels, Z_1 is positive. For the purpose of comparison, the vertical advection of mean potential vorticity by vertical cloud mass flux, $-M_c(\partial\bar{\chi}/\partial p)$, is also shown in the figure as the dashed line. The two curves are very similar in shape. However, this is somewhat misleading because the difference between the two curves is actually quite substantial in magnitude.

Since $\bar{Q}_R$ is much smaller than Q_1, while $L(\bar{c} - \bar{e})$ and Q_1 have comparable magnitudes, the contribution to Z_1 due to the mean radiation process can be

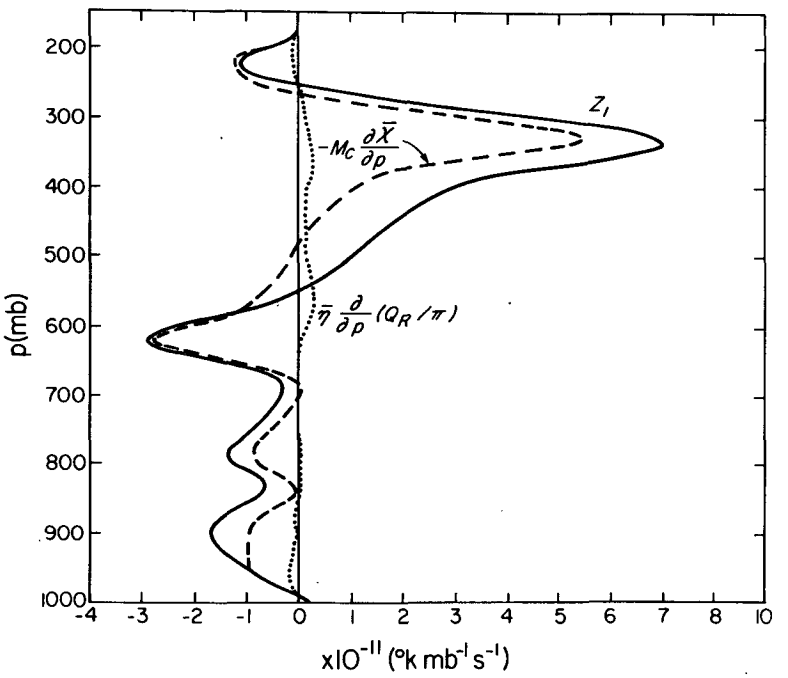

FIG. 7. GATE A/B-scale apparent potential vorticity source Z_1 for the period 0000–2400 GMT 2 September. Also shown as the dashed line is the vertical advection of mean potential vorticity by total cloud mass flux. The dotted line shows the radiation effect.

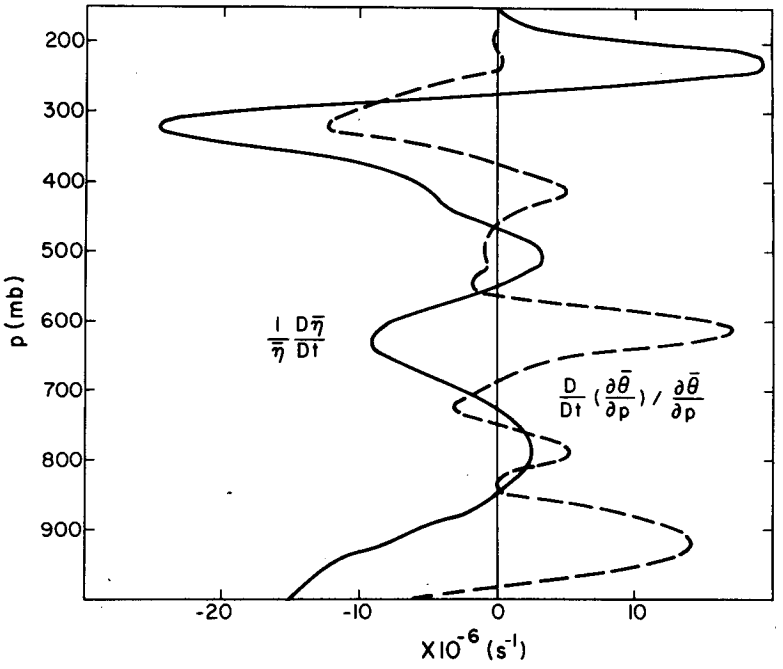

FIG. 8. The decomposition of the A/B-scale apparent potential vorticity source into a dynamic and a thermodynamic component according to Eq. (45) for the period 0000–2400 GMT 2 September.

expected to be small. The radiation terms in the Z_1 equation can also be written as

$$+\frac{\partial}{\partial p}(\bar{\eta}\bar{Q}_R/C_p\pi) - \frac{1}{\bar{\rho}g}\nabla_H\cdot(\bar{\xi}\bar{Q}_R/C_p\pi)$$

$$= \bar{\eta}\frac{\partial}{\partial p}(\bar{Q}_R/C_p\pi) - \frac{1}{\bar{\rho}g}\bar{\xi}\cdot\nabla_H(\bar{Q}_R/C_p\pi).$$

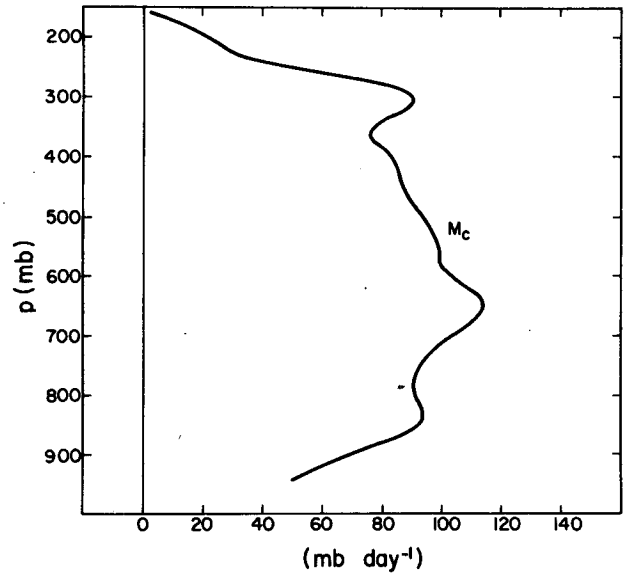

FIG. 9. GATE A/B-scale total cloud mass flux M_c for the 0000–2400 GMT 9 September period.

The vertical profile for the first term on the right-hand side of the above equation is plotted in Fig. 7 as the dotted line. Due to the difficulties in estimating the cloud amount and its spatial distribution for the radiation calculations, only a mean radiation profile has been calculated for the entire A/B-scale area. We have not been able to make any reliable estimates of the horizontal gradient of Q_R. The second term involving $\nabla_H\bar{Q}_R$ is therefore assumed to be zero. In view of the overall small effects of radiation, this assumption is not likely to introduce serious errors.

We note that the potential vorticity is a composite variable involving the potential temperature and the vorticity. The apparent potential vorticity source Z_1 therefore includes the dynamic effects as well as the thermodynamic effects of cumulus clouds. The potential vorticity equation can be a useful tool for the study and parameterization of the dynamic effects of cumulus clouds only if the thermodynamic effects of clouds are not so strong as to mask their dynamic effects in the potential vorticity budget. We shall use the observational data here to examine the problem.

If one adopts as a first approximation the approximate expression for $\bar{\chi}$ given by Eq. (44), it can readily be shown that

$$\frac{D\bar{\chi}}{Dt}\Big/\bar{\chi} = \frac{D\bar{\eta}}{Dt}\Big/\bar{\eta} + \frac{D}{Dt}\left(\frac{\partial\bar{\theta}}{\partial p}\right)\Big/\frac{\partial\bar{\theta}}{\partial p}, \quad (45)$$

where D/Dt is the total derivative. The first term on the right-hand side of the above equation can be interpreted as the fractional change of the large-scale mean potential vorticity due to the fractional change in the mean vorticity field, and the second term as the fractional change in $\bar{\chi}$ due to the change in the potential temperature field. The formulation presented in this study is useful for the study of dynamical effects of cumulus clouds only if the first term is at least of the same order of magnitude as the second term.

To estimate *a priori* the magnitude of these two terms, although possible, could be quite tedious. Instead, observational data will be used in this study to calculate the values of the two terms. Their magnitudes can then be compared readily. The results of the calculations are shown in Fig. 8. The two terms are of the order of $1-2 \times 10^{-5}$ s^{-1}. Overall, they contribute about equally to the large-scale potential vorticity budget.

b. 9 September period

GATE A/B-scale thermodynamic budgets for this period and the cloud ensemble properties deduced from them have been presented in Cho *et al.* (1979a). The results are very similar to those for the 2 September period and will not be repeated here except for the total cloud mass flux M_c which will be referred to in later discussions and therefore is reproduced in Fig. 9 for convenience.

The M_c profile shows that the total cloud mass flux increases with height in the layer between cloud base and 600 mb level. On the average, there is a net convergence of environmental air into clouds and this is the mean entrainment layer for the cloud population. Above 600 mb, M_c first decreases slowly up to 300 mb and then decreases rapidly above. On the average there is a net divergence of cloud air in the layer above 600 mb, and for the cloud population as a whole, this is the mean detrainment layer.

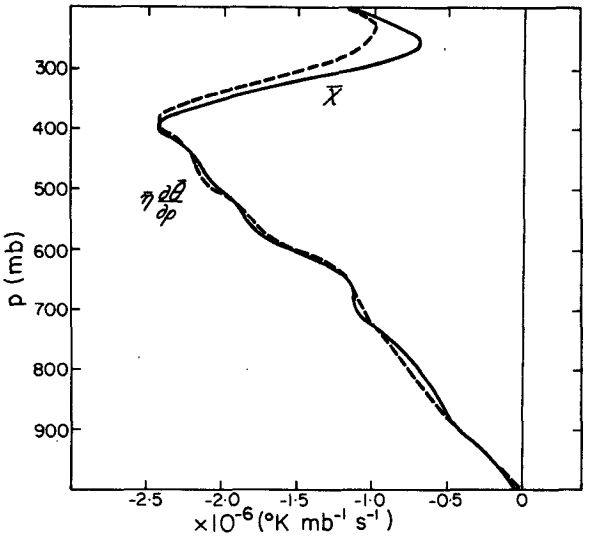

FIG. 10. As in Fig. 2 except for the 0000–2400 GMT 9 September period.

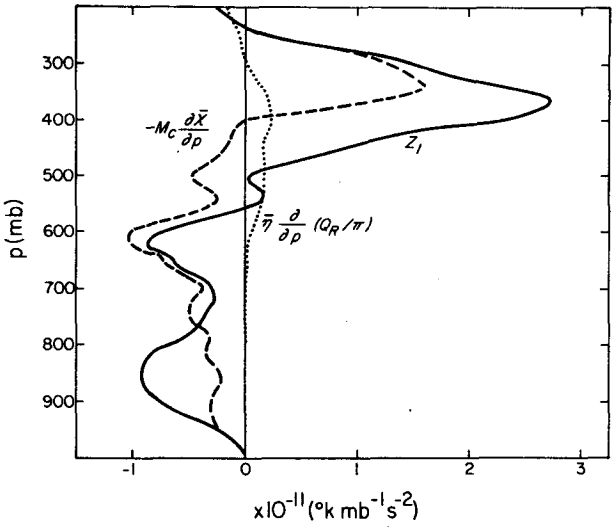

FIG. 11. As in Fig. 7 except for the 0000–2400 GMT 9 September period.

Having been discussed in Cho *et al.* (1979b), the recycling rate determined for this period shows negative values at around the 600 mb level. These negative values are physically unrealistic and are probably caused by data errors. In subsequent calculations, these negative values are removed and the calculated recycling rate profile below 500 mb are replaced by a smooth profile which gives the same total vertical integration.

The mean potential vorticity profile is shown in Fig. 10. Qualitatively, it is quite similar to that for the 2 September period. The apparent potential source Z_1 is shown in Fig. 11, and the decomposition of Z_1 into a thermodynamic and a dynamic component is presented in Fig. 12. These results again are quite similar to those for the 2 September period. The thermodynamic and the dynamic components contribute about equally to the observed potential vorticity source. The Z_1 profile shows a net potential porticity source above 500 mb and a net sink below. The dashed line in Fig. 11 shows the effect due to cloud vertical advection of mean potential vorticity for the purpose of comparison. The radiation effect is shown in the figure as the dotted line. The horizontal gradient of Q_R has been neglected, as in the 2 September period. Overall, the radiation effect is rather small.

8. The ensemble mean cloud vorticity

With the observed heat, moisture and potential vorticity budgets, the diagnostic method developed

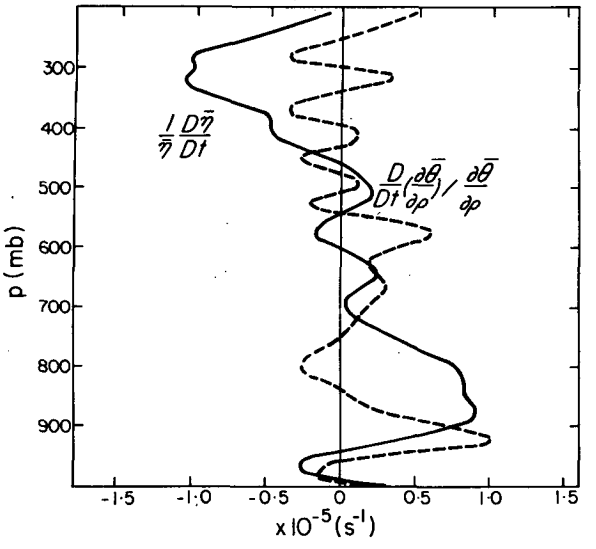

FIG. 12. As in Fig. 8 except for the 0000–2400 GMT 9 September period.

in Section 6 will now be used to determine the ensemble mean cloud vorticity.

The mean cloud potential vorticity $\bar{\chi}_c$ determined from the Z_1 budget through Eq. (30) for the 2 September period is shown in Fig. 13 as the dashed line. The large-scale potential vorticity $\bar{\chi}$ is also shown in the figure for comparison. The difference between $\bar{\chi}_c$ and $\bar{\chi}$ is quite substantial. The magnitude of $\bar{\chi}_c$ is smaller than $\bar{\chi}$ above 600 mb and larger than $\bar{\chi}$ below that level. This behavior of $\bar{\chi}_c$ can be explained only by considering the source term involving latent heating processes on the right-hand side of Eq. (29) or (32). Ignoring this source term, for example, a simple conservation of cloud potential vorticity, modified only by entrainment and detrainment processes, obviously cannot explain why the magnitude of mean cloud potential vorticity increases first more rapidly with height than does the environmental mean $\bar{\chi}$ above the cloud base and then decreases rapidly to values smaller than $\bar{\chi}$ above 600 mb. Note that at the cloud-base level $\bar{\chi}_c = \bar{\chi}$, as one would expect because at that level cloud air comes from the cloud environment where both the condensation and the evaporation rates of water substance are zero.

The mean cloud vorticity profiles determined through Eq. (34) for the 2 September period are shown in Fig. 14. For convenience we have plotted $\bar{\eta}_c - \bar{\eta}$, instead of $\bar{\eta}_c$ in the figure. The profiles I, II and III correspond to the three different assumptions of $\bar{\chi}_{cB}$ given by Eq. (43). Profile I is obtained by assuming that $\bar{\chi}_{cB} = \bar{\chi}_c$ at all levels, and profile II by assuming that $\bar{\chi}_{cB} = \bar{\chi}$. Profile III is obtained by assuming $\bar{\chi}_{cB} = \bar{\chi}_c$ in the mean cloud-detrainment layer, which is between 420 and 150 mb levels, as can be seen from the M_c profile shown in Fig. 4, and $\bar{\chi}_{cB} = \bar{\chi}$ in the mean cloud-entrainment layer which from the M_c profile is found to be between the cloud-base and the 420 mb height. The three $\bar{\eta}_c - \eta$ profiles are very similar qualitatively.

We note that $\bar{\eta}_c$ and $\bar{\eta}$ are generally of the same order of magnitude. All three profiles shown in the figure suggest that $\bar{\eta}_c$ is smaller than $\bar{\eta}$ in the mean cloud detrainment layer above 420 mb and larger than $\bar{\eta}$ in the mean cloud entrainment layer below. This result appears to be in agreement, qualitatively at least, with the simple mean cloud vorticity equation derived by Cho *et al.* (1979a):

$$\frac{\partial\bar{\eta}_c}{\partial t} = -\bar{\delta}_c\bar{\eta}_{cB}. \tag{46}$$

Here $\bar{\delta}_c$ is the mean cloud divergence and $\bar{\eta}_{cB}$ is the value of η_c averaged around the boundaries of clouds. Given the initial condition that $\bar{\eta}_c = \bar{\eta}$ and $\bar{\eta}_{cB} = \bar{\eta}$, a simple time integration of the above equation shows that $(\bar{\eta}_c - \bar{\eta})$ should be a positive quantity in the cloud entrainment layer because in the entrainment layer, the mean cloud divergence $\bar{\delta}_c$ is a negative quantity. On the other hand, $\bar{\delta}_c > 0$ in the cloud-detrainment layer and $\bar{\eta}_c$ should therefore be smaller than $\bar{\eta}$. A quantitative comparison between the diagnostically determined $\bar{\eta}_c$ and the solutions of Eq. (46) requires a detailed knowledge of the cloud distribution function and the cloud life span $\tau_{p'}$ as a function of maximum cloud-top height. No such an attempt will be made here because of lack of information about these quantities. Fraedrich (1974) suggested by analogy with the large-scale mean potential vorticity that the approximation

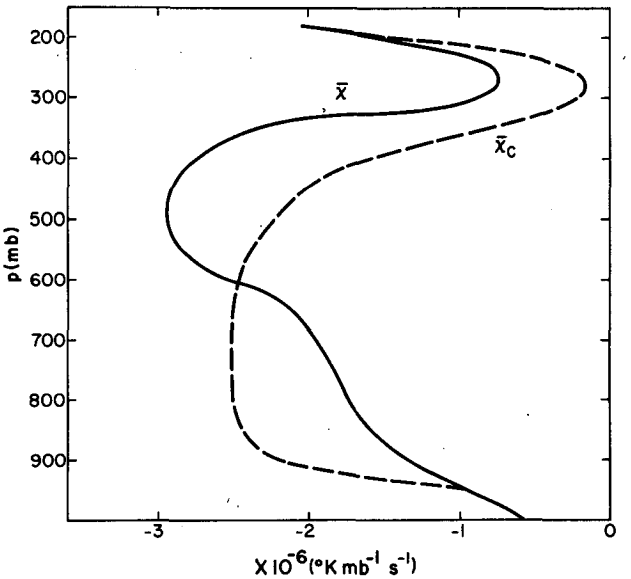

FIG. 13. GATE A/B-scale mean cloud potential vorticity $\bar{\chi}_c$ for the period 0000–2400 GMT 2 September.

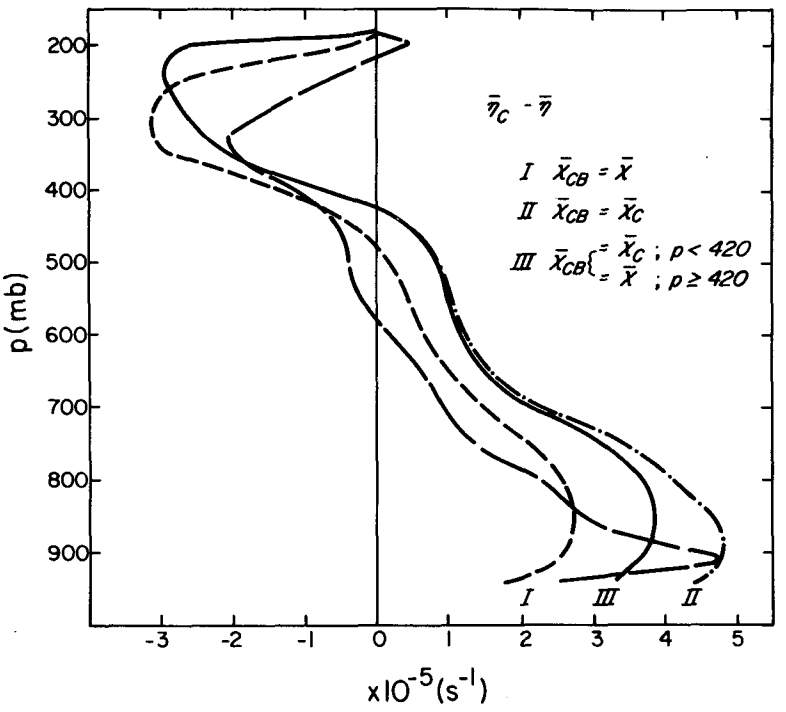

FIG. 14. The A/B-scale mean cloud vertical vorticity minus mean vertical vorticity profiles for the period 0000–2400 GMT 2 September. The three profiles I, II and III correspond to the three boundary conditions given in Eq. (43). The long-dashed line in the figure is the mean cloud vertical vorticity calculated from the mean cloud potential vorticity according to Eq. (47).

$$\bar{\chi}_c = \bar{\eta}_c \frac{\partial \bar{\theta}_c}{\partial p} \tag{47}$$

may be applied even to the cloud-scale potential vorticity field. The approximation is essential to the simplicity of the formulation derived by the author. No justifications, however, were given. [The potential vorticity was actually defined by the author in terms of moist static energy h, instead of potential temperature θ. The approximation corresponding to Eq. (47) was $\bar{\chi}_c = \bar{\eta}_c \partial \bar{h}_c / \partial p$. If the same degree of simplicity is to be achieved in the formulation presented in this paper, Eq. (47) is needed.]

In order to examine quantitatively the validity of this assumption we present in Fig. 14 the profile of

$$\bar{\chi}_c \left(\frac{\partial \bar{\theta}_c}{\partial p} \right)^{-1} - \bar{\eta}$$

as the long-dashed line. The result shows rather surprisingly that the approximation is acceptable not only qualitatively but also quantitatively. Within the range of uncertainties, the profile appears to agree with the $\bar{\eta}_c - \bar{\eta}$ profiles determined using our diagnostic method. We have no explanations, however, for this result at present.

The $\bar{\eta}_c - \bar{\eta}$ profiles determined for the 9 September period are shown in Fig. 15. The differences between the three profiles corresponding to the three boundary conditions are very small. The M_c profile for this period shown in Fig. 9 shows that the mean cloud entrainment layer is between the cloud base and the 650 mb level. In this layer, $\bar{\eta}_c$ is larger than $\bar{\eta}$. In the mean cloud-detrainment layer between 650 and 150 mb $\bar{\eta}_c$ is smaller than $\bar{\eta}$. These again are consistent with Eq. (46), as in the 2 September period.

9. Summary and conclusions

The concept of potential vorticity has been very useful in studying the dynamic processes in midlatitude circulation systems. In order to extend this conceptual tool to the study of motion systems in the tropical atmosphere, the effects of cumulus convection on the mean potential vorticity field must first be examined. We have presented in this paper some theoretical and observational results about these effects.

The results of our study have revealed that cumulus clouds modify the mean potential vorticity field not only through vertical mixing of potential vorticity, but also through the generation of potential vorticity by the release of latent heat. However, despite the strong thermodynamic effects due to latent heat release, the dynamic and thermodynamic

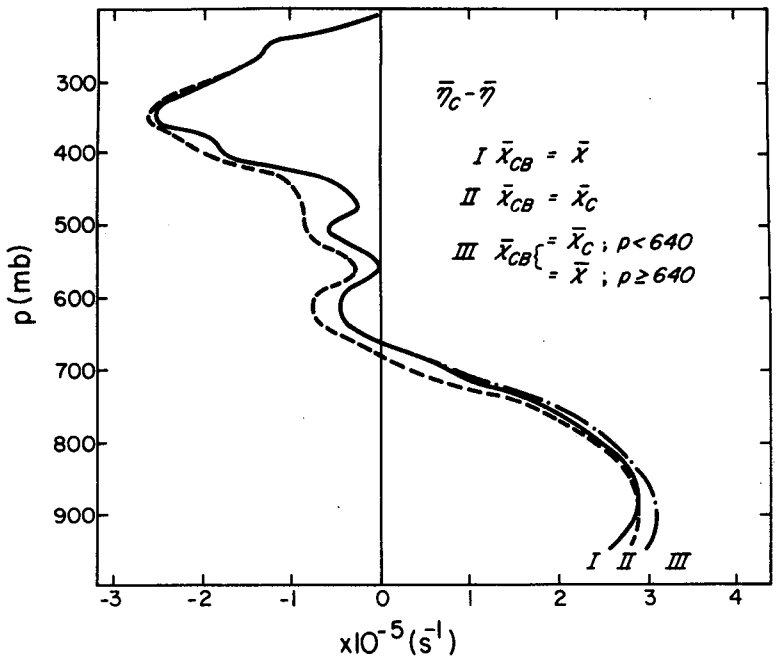

FIG. 15. As in Fig. 14 except for the period 0000–2400 GMT 9 September.

effects of cumulus cloud contribute about equally to the large-scale potential vorticity budget. This is very important if potential vorticity is to be used to describe the dynamic processes of the tropical atmosphere.

A diagnostic method has also been developed in this paper to determine the mean cloud vorticity field from the observed potential vorticity field. The method has been applied to two GATE A/B-scale potential vorticity budgets. The results show that 1) the mean cloud vorticity is of the same order of magnitude as the large-scale mean vorticity, despite the smallness of the horizontal scales of cumulus clouds, and 2) the mean cloud vorticity is smaller than the large-scale mean vorticity in the layer where there is a net divergence of cloud air into the cloud environment, and is larger than the large-scale mean vorticity in the layer where there is a net convergence of environmental air into clouds. These properties are in agreement with the analysis presented by Cho *et al.* (1979a).

The diagnostic results presented in this paper can also be useful for some other purposes. For example, Cho and Cheng (1979) have evaluated the effects of cloud horizontal eddy transport of vorticity on the large-scale vorticity budgets, using the mean cloud vorticity profiles determined in this paper. They have found that better agreements with observations are obtained if horizontal eddy transport of vorticity is included in their calculations. These calculations are now being extended to other periods of GATE.

Even though the results obtained in this study are generally quite gratifying, a few important questions remain unresolved. It is not clear from the results whether the horizontal eddy transport of potential vorticity is an important component in the mean potential vorticity budget. The mean cloud vorticity profiles determined with and without this effect of eddy transport are similar qualitatively, but they are somewhat different quantitatively in one of the periods analyzed (the 2 September period). It is also not clear whether the approximation given by Eq. (47) is acceptable for the cloud-scale potential vorticity, and for what reasons. A three-dimensional time-dependent cloud model will perhaps be needed to answer these questions.

Acknowledgments. The work was supported by the National Research Council of Canada through Grant A0601; and by the Atmospheric Environment Service, Department of Environment of Canada, through its Science Subvention Program. The authors wish to thank Miss Judy Brioux and Miss Janet Reith for typing the manuscript, and Drs. R. J. Reed, L. J. Shapiro and D. E. Stevens for useful comments and suggestions during the course of this work.

REFERENCES

Arakawa, A., and W. H. Schubert, 1974: Interaction of a cumulus cloud ensemble with the large-scale environment. Part I. *J. Atmos. Sci.*, **31**, 674–701.

Cho, H. R., 1977: Contribution of cumulus cloud life-cycle effects to the large-scale heat and moisture budget equations. *J. Atmos. Sci.*, **34**, 87–97.

——, and L. Cheng, 1979: Parameterization of horizontal transport of vorticity by cumulus convection. *J. Atmos. Sci.*, **37**, 812–826.

——, —— and R. M. Bloxam, 1979a: The representation of cumulus cloud effects in the large-scale vorticity equation. *J. Atmos. Sci.*, **36**, 127–139.

——, R. M. Bloxam, and L. Cheng, 1979b: GATE A/B-scale budget analysis. *Atmos. Ocean*, **17**, 60–76.

Fraedrich, K., 1974: Dynamic and thermodynamic aspects of the parameterization of cumulus convection. Part II, *J. Atmos. Sci.*, **31**, 1838–1849.

Nitta, T., 1977: Response of cumulus updraft and downdraft to GATE A/B-scale motion systems. *J. Atmos. Sci.*, **34**, 1163–1186.

Ogura, Y., and H. R. Cho, 1973: Diagnostic determination of cumulus cloud populations from observed large-scale variables. *J. Atmos. Sci.*, **30**, 1276–1286.

Ooyama, K., 1971: A theory of parameterization of cumulus convection. *J. Meteor. Soc. Japan*, **49**, 744–756.

Reed, R. J., and R. H. Johnson, 1974: The vorticity budget of synoptic-scale wave disturbances in the tropical western Pacific. *J. Atmos. Sci.*, **31**, 1784–1790.

Reeves, R. W., C. F. Ropelewski and M. D. Hudlow, 1979: Relationship between large-scale motion and convective precipitation during GATE. *Mon. Wea. Rev.*, **107**, 1154–1168.

Rogers, C. D., and S. D. Walshaw, 1966: The computation of infrared cooling rates in planetary atmosphere. *Quart. J. Roy. Meteor. Soc.*, **92**, 67–92.

Ruprecht, E., and W. Gray, 1976: Analysis of satellite-observed tropical cloud clusters. I. Wind and dynamic fields. *Tellus*, **28**, 391–413.

Shapiro, L. J., 1978: The vorticity budget of a composite African tropical wave disturbance. *Mon. Wea. Rev.*, **106**, 806–817.

Stevens, D. E., 1979: Vorticity, momentum and divergence budgets of synoptic-scale wave disturbances in the tropical eastern Atlantic. *Mon. Wea. Rev.*, **107**, 535–550.

Thompson, R. M., S. W. Payne, E. E. Recker and R. J. Reed, 1979: Structure and properties of synoptic-scale wave disturbances in the intertropical convergence zone of the eastern Atlantic. *J. Atmos. Sci.*, **36**, 53–72.

Williams, K. T., and W. M. Gray, 1973: Statistical analysis of satellite-observed trade wind cloud clusters in the western North Pacific. *Tellus*, **25**, 4, 313–336.

Yanai, M., and T. Nitta, 1967: Computation of vertical motion and vorticity budget in a Caribbean easterly wave. *J. Meteor. Soc. Japan*, **45**, 444–466.

——, S. Esbensen and J. H. Chu, 1973: Determination of bulk properties of tropical cloud clusters from large-scale heat and moisture budgets. *J. Atmos. Sci.*, **30**, 611–627.